



UNIVERSITY OF LEEDS

This is a repository copy of *Solving the inverse three-dimensional continuous model of electrical resistance tomography using the method of fundamental solutions and the Markov chain Monte Carlo approach.*

White Rose Research Online URL for this paper:
<http://eprints.whiterose.ac.uk/119001/>

Version: Accepted Version

Proceedings Paper:

Dyhoum, TE, Aykroyd, RG orcid.org/0000-0003-3700-0816 and Lesnic, D (2017) Solving the inverse three-dimensional continuous model of electrical resistance tomography using the method of fundamental solutions and the Markov chain Monte Carlo approach. In: Chappell, D, (ed.) Proceedings of the Eleventh UK Conference on Boundary Integral Methods (UKBIM11). Eleventh UK Conference on Boundary Integral Methods (UKBIM11), 10-11 Jul 2017, Nottingham, UK. Nottingham Trent University: Publications , pp. 43-52. ISBN 9780993111297

© 2017, the Author(s). This is an author produced version of a paper published in Proceedings of the Eleventh UK Conference on Boundary Integral Methods (UKBIM11).

Reuse

Unless indicated otherwise, fulltext items are protected by copyright with all rights reserved. The copyright exception in section 29 of the Copyright, Designs and Patents Act 1988 allows the making of a single copy solely for the purpose of non-commercial research or private study within the limits of fair dealing. The publisher or other rights-holder may allow further reproduction and re-use of this version - refer to the White Rose Research Online record for this item. Where records identify the publisher as the copyright holder, users can verify any specific terms of use on the publisher's website.

Takedown

If you consider content in White Rose Research Online to be in breach of UK law, please notify us by emailing eprints@whiterose.ac.uk including the URL of the record and the reason for the withdrawal request.



eprints@whiterose.ac.uk
<https://eprints.whiterose.ac.uk/>

Chapter 1

Solving the inverse three-dimensional continuous model of electrical resistance tomography using the method of fundamental solutions and the Markov chain Monte Carlo approach

T. E. Dyhoum^{1,2}, R. G. Aykroyd² and D. Lesnic¹

¹ Department of Applied Mathematics,
University of Leeds
Leeds, LS2 9JT, UK

² Department of Statistics,
University of Leeds
Leeds, LS2 9JT, UK

Abstract. *This paper discusses the three-dimensional continuous model of electrical resistance tomography for detecting rigid inclusions embedded in a bounded background medium. The mathematical model is governed by Laplace's equation subject to a homogeneous Dirichlet boundary condition on the unknown rigid inclusion and Cauchy data on the outer boundary. The forward solver uses the meshless method of fundamental solutions, which is a discrete variant of the single layer potential in the direct form of the boundary element method for harmonic functions, but with source points shifted outside the solution domain such that singularities in the fundamental solution are avoided. The inverse solution is based on the Bayesian approach and Markov chain Monte Carlo (MCMC) estimation technique. The MCMC is used not only for estimating the desirable model parameters, but also for uncertainty and reliability assessment. Numerical examples are investigated to demonstrate the effectiveness and the accuracy of the proposed approach.*

1.1 Introduction

The paper extends the previous two-dimensional computations of direct and inverse problems [1] to three dimensions. As a remarkable step towards solving the direct and the inverse complete-electrode model of ERT in three-dimensions, we will consider first the continuous model.

Prior to this study, three-dimensional rigid inclusions have been reconstructed in [2, 6, 7] by standard regularization schemes, where the method of fundamental solutions (MFS) was used to produce the direct solution and a constrained optimization procedure was employed to determine the boundary of a three-dimensional star-shaped rigid inclusion. In this paper, we use the Bayesian statistical approach, instead of the gradient-based minimization of [2].

1.2 Main problems

We consider Laplace's equation

$$\Delta u = 0 \quad \text{in } \Omega, \quad (1.1)$$

in various geometries $\Omega \subset \mathbb{R}^3$.

Problem 1: We consider an annular domain $\Omega = \Omega_{Outer} \setminus \overline{\Omega}_{Inner}$ with a rigid inclusion

(a)

$$\Omega_{Inner} = \{(x, y, z) \in \mathbb{R}^3 \mid x^2 + y^2 + z^2 < (0.5)^2\} \quad (\text{a sphere}) \quad (1.2)$$

or

(b)

$$\Omega_{Inner} = \left\{ (x, y, z) \in \mathbb{R}^3 \mid \frac{x^2}{(0.5)^2} + \frac{y^2}{(0.5)^2} + \frac{z^2}{(0.4)^2} < 1 \right\} \quad (\text{an ellipsoid}) \quad (1.3)$$

inside the unit sphere $\Omega_{Outer} = \{(x, y, z) \in \mathbb{R}^3 \mid x^2 + y^2 + z^2 < 1\}$. Equation (1.1) is solved subject to the Dirichlet boundary conditions

$$u = f \quad \text{on } \partial\Omega_{Outer} \quad (1.4)$$

and

$$u = 0 \quad \text{on } \partial\Omega_{Inner}. \quad (1.5)$$

On the other hand, in the inverse formulation, since the concern is not only to find the potential u but also to reconstruct the rigid inclusion Ω_{Inner} , the following Neumann current flux measurement is required to compensate for the unknown geometry:

$$\frac{\partial u}{\partial n} = g \quad \text{on } \partial\Omega_{Outer}. \quad (1.6)$$

As a result, the inverse problem of the continuous model of ERT is given by equations (1.1) and (1.4)-(1.6). Uniqueness of this problem when $f \not\equiv 0$ and Ω is connected is provided in [5].

Problem 2: We consider the domain $\Omega = \Omega_{Outer} \setminus (\overline{\Omega}_{Inner1} \cup \overline{\Omega}_{Inner2})$ with two disjoint rigid inclusions, which need to be detected when the inverse problem is solved, given by

$$\begin{aligned} \Omega_{Inner1} &= \{(x, y, z) \in \mathbb{R}^3 \mid x^2 + (y - 0.5)^2 + z^2 < (0.4)^2\}, \\ \Omega_{Inner2} &= \{(x, y, z) \in \mathbb{R}^3 \mid x^2 + (y + 0.5)^2 + z^2 < (0.4)^2\}. \end{aligned} \quad (1.7)$$

These are located inside the unit sphere. Then, (1.1) is solved subject to (1.4), (1.6) and

$$u = 0 \quad \text{on } \partial\Omega_{Inner1} \cup \partial\Omega_{Inner2}. \quad (1.8)$$

1.3 The MFS for the direct problem

1.3.1 Mathematical formulation

The MFS seeks an approximation to the solution of (1.1) in a bounded domain with a rigid inclusion inside, as in (a) or (b), as a linear combination of fundamental solutions in the form

$$u(\underline{p}) = \sum_{k=1}^{2(N-1)} \sum_{l=1}^N c_{k,l} G(\underline{\xi}_{k,l}, \underline{p}), \quad \underline{p} \in \overline{\Omega}, \quad (1.9)$$

where $\underline{\xi}_{k,l}$ are source points located outside $\overline{\Omega}$ and G is the fundamental solution of the three-dimensional Laplace equation given by

$$G(\underline{\xi}, \underline{p}) = \frac{1}{4\pi|\underline{\xi} - \underline{p}|}. \quad (1.10)$$

The expression (1.9) results from the discretisation of a single-layer boundary integral representation of the harmonic function u with sources located outside the surface $\partial\Omega$.

The internal source points are located inside the inner domain Ω_{Inner} , and are defined, for Problem 1(a), by

$$\underline{\xi}_{k,l} = 0.5 \eta_I \left(\sin \tilde{\theta}_k \cos \tilde{\phi}_l, \sin \tilde{\theta}_k \sin \tilde{\phi}_l, \cos \tilde{\theta}_k \right), \quad k = \overline{1, (N-1)}, \quad l = \overline{1, N}, \quad (1.11)$$

where $0 < \eta_I < 1$ (η_I is a contraction parameter), and, for Problem 1(b), by

$$\underline{\xi}_{k,l} = \eta_I \left(0.5 \sin \tilde{\theta}_k \cos \tilde{\phi}_l, 0.5 \sin \tilde{\theta}_k \sin \tilde{\phi}_l, 0.4 \cos \tilde{\theta}_k \right), \quad k = \overline{1, (N-1)}, \quad l = \overline{1, N}, \quad (1.12)$$

$$\tilde{\theta}_k = \frac{\pi k}{N}, \quad k = \overline{1, (N-1)}, \quad \tilde{\phi}_l = \frac{2\pi(l-1)}{N}, \quad l = \overline{1, N}.$$

The external source points are located outside the outer domain Ω_{Outer} , and are defined (for both Problems 1(a) and 1(b)) by

$$\underline{\xi}_{k,l} = R \left(\sin \tilde{\theta}_{k-N+1} \cos \tilde{\phi}_l, \sin \tilde{\theta}_{k-N+1} \sin \tilde{\phi}_l, \cos \tilde{\theta}_{k-N+1} \right), \quad k = \overline{N, 2(N-1)}, \quad l = \overline{1, N}, \quad (1.13)$$

where $1 < R < \infty$. Similarly, the internal boundary collocation points are located on $\partial\Omega_{Inner}$, and are defined, for Problem 1(a), by

$$\underline{x}_{i,j} = 0.5 \left(\sin \theta_i \cos \phi_j, \sin \theta_i \sin \phi_j, \cos \theta_i \right), \quad i = \overline{1, (M-1)}, \quad j = \overline{1, M}, \quad (1.14)$$

and, for Problem 1(b), by

$$\underline{x}_{i,j} = \left(0.5 \sin \theta_i \cos \phi_j, 0.5 \sin \theta_i \sin \phi_j, 0.4 \cos \theta_i \right), \quad i = \overline{1, (M-1)}, \quad j = \overline{1, M}, \quad (1.15)$$

where

$$\theta_i = \frac{\pi i}{M}, \quad i = \overline{1, (M-1)}, \quad \phi_j = \frac{2\pi(j-1)}{M}, \quad j = \overline{1, M}.$$

The external boundary collocation points are located on $\partial\Omega_{Outer}$, and are defined (for both Problems 1(a) and 1(b)) by

$$\underline{x}_{i,j} = \left(\sin \theta_{i-M+1} \cos \phi_j, \sin \theta_{i-M+1} \sin \phi_j, \cos \theta_{i-M+1} \right), \quad i = \overline{M, 2(M-1)}, \quad j = \overline{1, M}. \quad (1.16)$$

In order to obtain the coefficient $\underline{c} = (c_{k,l})_{k=1,2(N-1), l=1,N}$, (1.9) is substituted into the boundary conditions (1.4) and (1.5). This results in

$$\sum_{k=1}^{2(N-1)} \sum_{l=1}^N G_{i,j,k,l} c_{k,l} = f_{i,j}, \quad i = \overline{1, 2(M-1)}, \quad j = \overline{1, M}, \quad (1.17)$$

where $f_{i,j} = f(\underline{x}_{i,j})$ and $G_{ijkl} = \frac{1}{4\pi|\underline{x}_{k,l} - \underline{x}_{i,j}|}$ for $i = \overline{1, 2(M-1)}$, $j = \overline{1, M}$, $k = \overline{1, 2(N-1)}$ and $l = \overline{1, N}$. Note that from (1.5), $f_{i,j} = 0$ for $i = \overline{1, (M-1)}$, $j = \overline{1, M}$. The linear system of algebraic equations (1.17) consists of $2(M-1) \times M$ equations with $2(N-1) \times N$ unknowns. If $M = N$, we can apply the Gaussian elimination method to obtain the MFS coefficients \underline{c} . If $M > N$ the least-squares method is used to solve the over-determined system of equations (1.17). Once the coefficient vector \underline{c} has been obtained accurately, equation (1.9) provides explicitly the solution for the potential u inside the domain Ω and, by differentiation, the current flux $\partial u / \partial n$ on the boundary $\partial\Omega$.

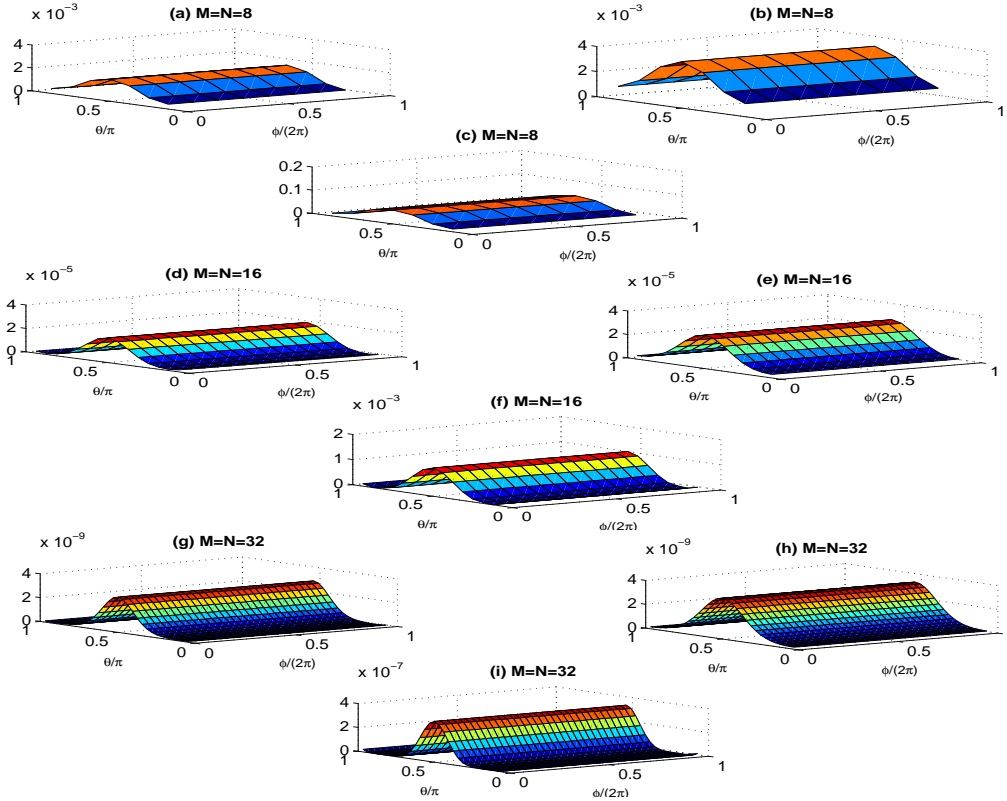


Figure 1.1: (a, d, g) The absolute errors between the MFS and exact interior solutions $u^{MFS}(0.6, \theta, \phi)$ and $u^{Exact}(0.6, \theta, \phi)$, (b, e, h) the absolute errors between the MFS and exact outer derivative $(\partial u / \partial n)^{MFS}(1, \theta, \phi)$ and $(\partial u / \partial n)^{Exact}(1, \theta, \phi)$, and (c, f, i) the absolute errors between the MFS and exact inner derivative $(\partial u / \partial n)^{MFS}(0.5, \theta, \phi)$ and $(\partial u / \partial n)^{Exact}(0.5, \theta, \phi)$, for $M = N = \{8, 16, 32\}$, as functions of $\phi/(2\pi)$ and θ/π .

1.3.2 Numerical results

Example 1: Solve, using the MFS, the direct problem 1(a) given by (1.1), (1.4) with $f = -1$, and (1.5) which has the analytical solution given by

$$u(x, y, z) = \frac{1}{\sqrt{x^2 + y^2 + z^2}} - \frac{1}{0.5}, \quad (x, y, z) \in \Omega. \quad (1.18)$$

Solution: Choosing $M = N = 16$ results in $30 \times 16 = 480$ boundary collocation points and 480 source points. We also take $R = 5$ and $\eta_I = 0.6$.

Figure 1.1 illustrates the absolute errors between the exact and the numerical MFS solutions for various values of $M = N \in \{8, 16, 32\}$. From this figure, it can be seen that as $M = N$ increases, the accuracy of MFS solution increases.

Example 2: Consider the numerical solution of the direct problem 2 given by (1.1), (1.4), (1.7) and (1.8) using the MFS when

$$f(x, y, z) = x^2 + y^2 - 2z^2, \quad (x, y, z) \in \partial\Omega_{Outer}. \quad (1.19)$$

Note that in this case an analytical solution is not available. The MFS implementation requires some changes when the two inclusions (1.7) are present but these are straight forward.

Solution: Choosing $M = N = 16$ results in $45 \times 16 = 720$ collocation points and 720 source points. We also take $R = 5$ and $\eta_I = 0.6$.

Figure 1.2 illustrates the rapid convergence of the MFS numerical normal derivative on the external boundary $\partial\Omega_{Outer}$ for various $M = N = \{8, 16, 32, 64\}$. It is also obvious that the two peaks are caused by the existence of the two inner rigid inclusions (1.7).

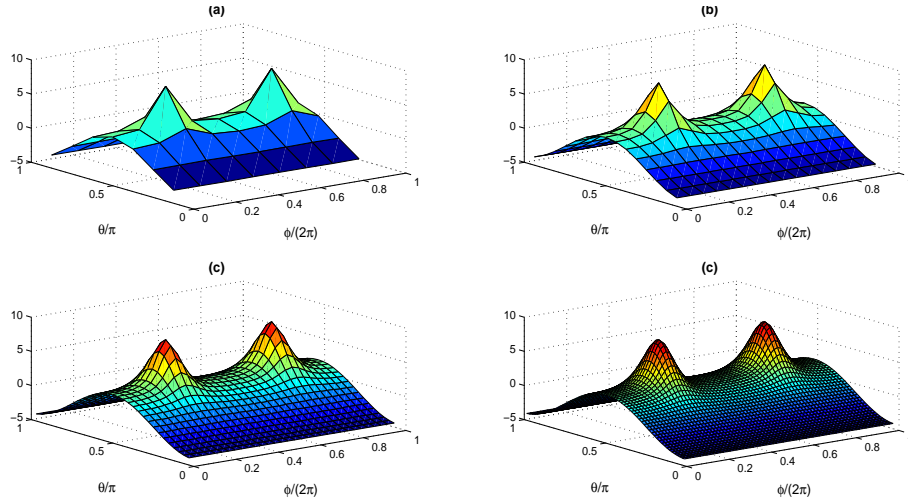


Figure 1.2: The MFS outer derivative $(\partial u / \partial n)_{Outer}^{MFS}(1, \theta, \phi)$, as a function of $\phi/(2\pi)$ and θ/π , for (a) $M = N = 8$, (b) $M = N = 16$, (c) $M = N = 32$, (d) $M = N = 64$, when $R = 5$ and $\eta_I = 0.6$.

1.4 The inverse solution in three dimensions

1.4.1 One rigid inclusion (inverse problems 1(a) and 1(b))

Consider a three-dimensional star-shaped object Ω_{Inner} centered at the origin in the unit sphere Ω_{Outer} and parametrised by

$$r_{i,j} = r(\tilde{\theta}_i, \tilde{\phi}_j), \quad i = \overline{1, (N-1)}, \quad j = \overline{1, N}, \quad (1.20)$$

using the spherical coordinates representation

$$\Omega_{Inner} = \{r(\theta, \phi) (\sin \theta \cos \phi, \sin \theta \sin \phi, \cos \theta) \mid \phi \in [0, 2\pi), \theta \in (0, \pi)\}. \quad (1.21)$$

The boundary potential u is specified as in (1.4) and the current flux $\partial u / \partial n$ is obtained numerically by solving the direct problem in order to provide the current flux data (1.6). Afterwards, the potential and current flux values are corrupted with noise as

$$w_{i,j} = f(x_{i,j}) + \eta_{i,j}, \quad v_{i,j} = g(x_{i,j}) + \zeta_{i,j}, \quad i = \overline{M, 2(M-1)}, \quad j = \overline{1, M}, \quad (1.22)$$

where the additive noise variables $\eta_{i,j}$ and $\zeta_{i,j}$ follow independent Gaussian distributions with zero means and variances σ_w^2 and σ_v^2 , respectively.

Based on (1.9), (1.20) and (1.21), the rigid-inclusion condition (1.5) is imposed as

$$\sum_{k=1}^{2(N-1)} \sum_{l=1}^N c_{k,l} G(\underline{\xi}_{k,l}, r_{i,j}(\sin \tilde{\theta}_i \cos \tilde{\phi}_j, \sin \tilde{\theta}_i \sin \tilde{\phi}_j, \cos \tilde{\theta}_i)) = 0, \quad i = \overline{1, (N-1)}, \quad j = \overline{1, N}. \quad (1.23)$$

Also, (1.4) and (1.6) yield

$$\sum_{k=1}^{2(N-1)} \sum_{l=1}^N c_{k,l} G(\underline{\xi}_{k,l}, \underline{x}_{i,j}) = w_{i,j}, \quad i = \overline{M, 2(M-1)}, \quad j = \overline{1, M}, \quad (1.24)$$

$$\sum_{k=1}^{2(N-1)} \sum_{l=1}^N c_{k,l} \frac{\partial G}{\partial n}(\underline{\xi}_{k,l}, \underline{x}_{i,j}) = v_{i,j}, \quad i = \overline{M, 2(M-1)}, \quad j = \overline{1, M}. \quad (1.25)$$

Equations (1.23)-(1.25) create a nonlinear system of $(N-1) \times N + 2(M-1) \times M$ equations with $3(N-1) \times N$ unknowns given by the radii $\underline{r} = (r_{i,j})$ for $i = \overline{1, (M-1)}, j = \overline{1, N}$ and the MFS coefficients $\underline{c} = (c_{k,l})$ for $k = \overline{1, 2(M-1)}, l = \overline{1, N}$. Although the linearity in \underline{c} is obvious in equations (1.24) and (1.25), equation (1.23) clearly shows the nonlinearity between \underline{r} and \underline{c} .

The constraint $0 < r_{ij} < 1$ for $i = \overline{1, (N-1)}, j = \overline{1, N}$ is imposed to ensure that the inner star-shaped object remains within the unit sphere during the reconstruction process.

1.4.2 Two rigid inclusions (inverse problem 2)

Now consider two three-dimensional star-shaped objects Ω_{Inner1} and Ω_{Inner2} centered at given points say, (X_0, Y_0, Z_0) and (X_1, Y_1, Z_1) in the unit sphere Ω_{Outer} and represented by $\underline{r}_1 = (r_{i,j}^1)_{i=\overline{1, (N-1)}, j=\overline{1, N}}$ and $\underline{r}_2 = (r_{i,j}^2)_{i=\overline{1, (N-1)}, j=\overline{1, N}}$, respectively, defined as in (1.20).

Conditions (1.8), (1.4) and (1.6) are

$$\sum_{k=1}^{3(N-1)} \sum_{l=1}^N c_{k,l} G(\underline{\xi}_{k,l}, r_{i,j}(\sin \tilde{\theta}_i \cos \tilde{\phi}_j, \sin \tilde{\theta}_i \sin \tilde{\phi}_j, \cos \tilde{\theta}_i)) = 0, \quad i = \overline{1, 2(N-1)}, \quad j = \overline{1, N}. \quad (1.26)$$

$$\sum_{k=1}^{3(N-1)} \sum_{l=1}^N c_{k,l} G(\underline{\xi}_{k,l}, \underline{x}_{i,j}) = w_{i,j}, \quad i = \overline{(2(M-1)+1), 3(M-1)}, \quad j = \overline{1, M}, \quad (1.27)$$

$$\sum_{k=1}^{3(N-1)} \sum_{l=1}^N c_{k,l} \frac{\partial G}{\partial n}(\underline{\xi}_{k,l}, \underline{x}_{i,j}) = v_{i,j}, \quad i = \overline{(2(M-1)+1), 2(M-1)}, \quad j = \overline{1, M}. \quad (1.28)$$

Equations (1.26)-(1.28) create a nonlinear system of $2(N-1) \times N + 2(M-1) \times M$ equations with $5(N-1) \times N$ unknowns. We also need to take into account that the distance between the centres is greater than the sum of the diameters, namely,

$$S = \sqrt{(X_0 - X_1)^2 + (Y_0 - Y_1)^2 + (Z_0 - Z_1)^2} > \text{diam}(\Omega_{Inner_1}) + \text{diam}(\Omega_{Inner_2}), \quad (1.29)$$

where the diameters of Ω_{Inner_1} and Ω_{Inner_2} are defined as

$$\text{diam}(\Omega_{Inner_i}) = \max_{\underline{x}, \underline{y} \in \partial\Omega_{Inner_i}} |\underline{x} - \underline{y}|, \quad i = 1, 2. \quad (1.30)$$

1.4.3 Statistical approach

The solution of the inverse problem (1.23)-(1.25) or (1.26)-(1.28) is obtained using the MCMC, as described in [1, 4]. Due to the ill-posedness and non-linearity of the ERT inverse problem, we consider the Bayesian approach which is linked to Markov chain Monte Carlo (MCMC) algorithms to work as a regularization scheme interpreted in terms of prior information. Modelling the prior information is a very important process in order to obtain reliable conclusions about the solution.

The main ingredients in the Bayesian statistical framework are the likelihood function and a prior distribution which describes the model parameters before the data is considered. The product of the likelihood function and the prior distribution, an application of Bayes theorem, leads to the posterior distribution (the solution of the inverse problem), see [4] for more details. In the inverse problem, the model parameters which must be estimated using the potential and current flux data, are the MFS coefficients \underline{c} and the radii \underline{r} . These are high-dimensional parameters, for both inverse problems considered in this paper, which make the posterior distribution complicated to solve numerically using standard methods. This is why the MCMC technique is used in this paper to estimate the shape and the size of the inner rigid inclusions. Another advantage of using MCMC is that it also allows deeper understanding of the posterior distribution in terms of accuracy and reliability, for example by calculation of credible intervals of the unknown parameters, [1, 4].

Although the MCMC offers a flexible tool to fully investigate the reliability and quantify uncertainty of the posterior distribution, it makes intensive use of the forward solver which can be a drawback especially when three-dimensional ERT problems are being solved. Hence, using a meshless method, such as the MFS described in the previous subsections, is more advantageous than using domain or boundary discretisation methods.

The type of MCMC technique which is used here is the Metropolis-Hastings algorithm where the initial guess of the radii is selected by finding a well-fitting circle for the inner inclusion and the initial values for the MFS coefficients are chosen to be zero. For more details of similar use of MCMC see [1, 3, 4].

1.4.4 Numerical results and discussion

Experiment 1. Find the inverse solution of Problem 1(a) satisfying (1.1) and (1.4), with $f = -1$, and (1.5) by fitting a star-shaped object model using the data (1.6) from a spherical inclusion (a) of radius 0.5 centred at $(0, 0, 0)$.

First of all, the current flux $\partial u / \partial n$ on the external boundary $\partial\Omega_{Outer}$, is calculated numerically by solving the forward Dirichlet problem (1.1), (1.4) and (1.5) using the MFS with

$(N - 1)N = 35 \times 36 = 1260$. Then, (1.22) is considered on a set of equally-spaced collocation points, with $(M - 1)M = 13 \times 14 = 182$, on the external fixed boundary $\partial\Omega_{Outer}$. We add noise to those boundary measurements with a standard deviation $\sigma_w = \sigma_v = 0.01$.

We take $(N - 1)N = 14 \times 15 = 210$ which makes the discretised problem (that defined in (1.23)-(1.25)) under-determined, since it consists of $(N - 1)N + 2(M - 1)M = 210 + 2 \times 182 = 574$ equations with $3(N - 1)N = 3 \times 210 = 630$ unknowns. We take $\eta_I = 0.6$ and $R = 5$.

Secondly, the hierarchical structure of the statistical model in [1] is considered. The values of the hyper-prior parameters of the internal and external MFS coefficients are fixed at $\alpha_{C_I} = 0.0116$ and $\alpha_{C_E} = 0.2457$, respectively, as well as the hyper-prior parameter value for the radius at $\alpha_r = 0.1$ (based on previous work [1, 3]).

It can be seen from Table 1.1 that as the number K of MCMC iterations increases, the three-dimensional reconstruction for the star-shaped model (1.20) become better. This is due to the average of corresponding estimated radii becoming closer to the true value which is 0.5 and its standard deviation (given in brackets) is much smaller.

K	The estimated radius	The standard deviation
5	0.4895	0.0153
10	0.4888	0.0103
20	0.4926	0.0178
40	0.4968	0.0094

Table 1.1: The average of the estimated radii with the corresponding standard deviations, for Experiment 1, for various iterations $K \in \{5, 10, 20, 40\}$.

Experiment 2. Find the inverse solution of Problem 1(b) by fitting a star-shaped object model using the data from an ellipsoid inclusion of radius given by

$$r(\theta, \phi) = \sqrt{(0.5 \sin \theta \cos \phi)^2 + (0.5 \sin \theta \sin \phi)^2 + (0.4 \cos \theta)^2}, \quad \theta \in (0, \pi), \quad \phi \in [0, 2\pi). \quad (1.31)$$

The Dirichlet data (1.4) on $\partial\Omega_{Outer}$ is taken as

$$u(x, y, z) = f(x, y, z) = e^{x+y}, \quad (x, y, z) \in \partial\Omega_{Outer}. \quad (1.32)$$

Figure 1.3 shows an excellent three-dimensional reconstruction for the ellipsoid (1.31). The MCMC algorithm converges to the exact ellipsoid within just a few iterations with a run time, for $K = 80$, of about three hours.

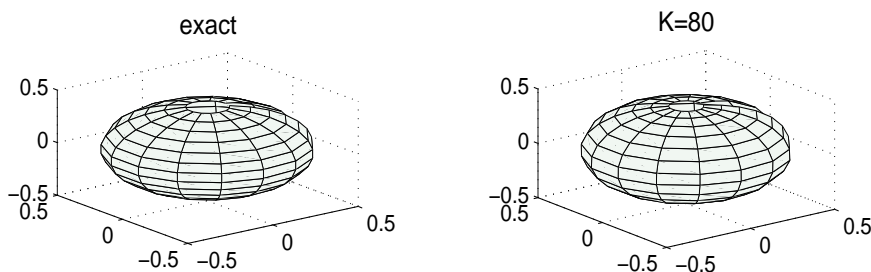


Figure 1.3: Star-shaped model reconstruction: The exact inner ellipsoid and the fitted ellipsoids after $K = 80$ iterations.

One way to illustrate that the MCMC works well is to consider the 2-norm values of $(r_{i,j}^{MFS} - r_{i,j}^{exact})$, $i = \overline{1,14}$, $j = \overline{1,15}$, as well as the maximum absolute error values for

$K \in \{5, 10, 20, 40, 80\}$, see Table 1.2. The random fluctuations suggest that the MCMC algorithm is in equilibrium and mixing well.

K	$\ r_{i,j}^{MFS} - r_{i,j}^{exact}\ $	$\max r_{i,j}^{MFS} - r_{i,j}^{exact} $
5	0.0068	0.0063
10	0.0053	0.0036
20	0.0066	0.0036
40	0.0086	0.0052
80	0.0084	0.0031
160	0.0102	0.0028
320	0.0168	0.0047

Table 1.2: The 2-norm of $(r_{i,j}^{MFS} - r_{i,j}^{exact})$, $i = \overline{1,14}$, $j = \overline{1,15}$, and the maximum absolute error, for Experiment 2, for various $K \in \{5, 10, 20, 40, 80, 160, 320\}$.

A better way to illustrate the reliability of the MCMC algorithm is to plot, see Figure 1.4, the object boundary credible intervals for some cross-sections in the xy -plane of the three-dimensional reconstruction. From this figure, it can be seen that the width of the credible intervals is very narrow near the top and the bottom of the reconstructed ellipsoid compared to the ones at the middle due to the data distribution.

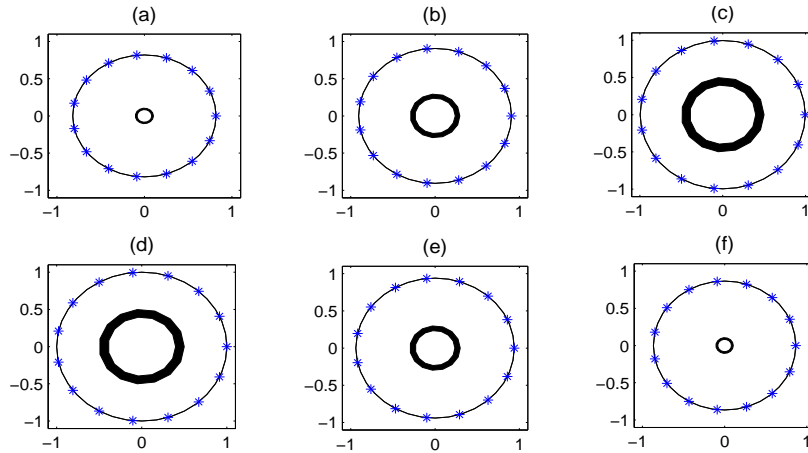


Figure 1.4: Credible intervals for various cross-sections (a) $\theta = \frac{\pi}{14}$, (b) $\theta = \frac{3\pi}{14}$, (c) $\theta = \frac{6\pi}{14}$, (d) $\theta = \frac{8\pi}{14}$, (e) $\theta = \frac{11\pi}{14}$, and (f) $\theta = \frac{13\pi}{14}$ and $(\phi)_{j=\overline{1,15}} \in [0, 2\pi)$, for Experiment 2.

Experiment 3. Find the inverse solution of Problem 2 satisfying (1.1), (1.4) with f given by (1.32) and (1.8) by fitting a star-shaped object model using the data (1.6) from two spherical inclusions (1.7) of radii 0.4 centred at $(0, 0.5, 0)$ and $(0, -0.5, 0)$.

Firstly, the current flux $\partial u / \partial n$ is calculated numerically on the external boundary $\partial\Omega_{Outer}$ by solving the forward Dirichlet problem (1.1), (1.4), (1.7) and (1.8) using the MFS with the same inputs as in Experiment 1. Note that in the inverse problem, by extending the number of rigid inclusions to two leads to a greater number of equations, $2(N-1)N + 2(M-1)M = 2 \times 210 + 2 \times 210 = 840$ equations with $5(N-1)N = 5 \times 210 = 1050$ unknowns.

Figure 1.5 shows the credible intervals over some selected cross-sections of the three-dimensional reconstructions confirming the solution's reliability.

1.5 Conclusion

The MFS has been successfully employed in combination with the MCMC to solve the three-dimensional inverse problem in the continuous model of ERT. The combined method has successfully detected three-dimensional star-shaped rigid inclusions (single sphere and ellipsoid, and two spheres). This was further justified by producing and interpreting cross-sections of credible intervals for the inner radii. Further work will consider reconstructing rigid inclusions from voltage measurements resulted from the three-dimensional complete-electrode model of ERT.

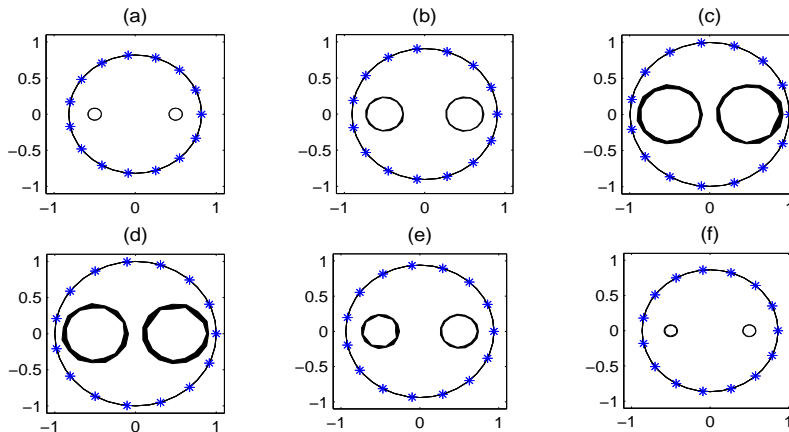


Figure 1.5: Credible intervals for various cross-sections (a) $\theta = \frac{\pi}{14}$, (b) $\theta = \frac{3\pi}{14}$, (c) $\theta = \frac{6\pi}{14}$, (d) $\theta = \frac{8\pi}{14}$, (e) $\theta = \frac{11\pi}{14}$, and (f) $\theta = \frac{13\pi}{14}$ and $(\phi)_{j=1,15} \in [0, 2\pi)$, for Experiment 3.

References

- [1] R. G. AYKROYD, D. LESNIC AND A. KARAGEORGHIS, *A fully Bayesian approach to shape estimation of objects from tomography data using MFS forward solutions*, Int. J. Tomography Simul., **28** (2015), 1-21.
- [2] D. J. BORMAN, D. B. INGHAM, B. T. JOHANSSON AND D. LESNIC, *The method of fundamental solutions for detection of cavities in EIT*, J. Integral Equations Appl., **21** (2009), 381-404.
- [3] T. E. DYHOUM, D. LESNIC AND R. G. AYKROYD, *Solving the complete-electrode direct model of ERT using the boundary element method and the method of fundamental solutions*, Electronic J. of Boundary Elements, **12** (2014), 26-71.
- [4] T. E. DYHOUM, R. G. AYKROYD AND D. LESNIC, *Reconstructing rigid inclusions in the complete-electrode model of ERT*. In: *Inverse Problems and Computational Mechanics*, Chapter 4, (eds. L. Marin, L. Munteanu and V. Chiroiu), 75-104, 2016.
- [5] H. HADDAR AND R. KRESS, *Conformal mappings and inverse boundary value problems*, Inverse Problems, **21** (2005), 935-953.
- [6] A. KARAGEORGHIS, D. LESNIC AND L. MARIN, *A moving pseudo-boundary MFS for three-dimensional void detection*, Adv. Appl. Math. Mech., **5** (2013), 510-527.
- [7] P. SERRANHO, *A hybrid method for inverse scattering for sound-soft obstacles in \mathbb{R}^3* , Inverse Problems Imaging, **1** (2007), 691-712.